**SERBIAN JOURNAL OF ELECTRICAL ENGINEERING**
**Vol. 19, No. 3, Ocotber 2022, 329-349**

**UDC: 621.316.936:621.33]:519.16** **DOI: https://doi.org/10.2298/SJEE2203329J**

# Optimal Siting of Capacitors in Distribution Grids Considering Electric Vehicle Load Growth Using Improved Flower Pollination Algorithm

**Varaprasad Janamala**[1]

**Abstract:** The optimal VAr compensation using capacitor banks (CBs) in radial distribution networks (RDNs) is solved in this paper while taking the growth of the load from electric vehicles (EVs) into consideration. This is accomplished by adapting an improved variant of the flower pollination algorithm (IFPA) with an enhanced local search capability. The primary objective of determining the locations and sizes of CBs is to minimize the distribution losses in the operation and control of RDNs. Additionally, the effect of CBs is shown by the increased net savings, greater voltage stability, and improved voltage profile. A voltage stability index (VSI) was used in the optimization process to determine the predefined search space for CB locations, and a double-direction learning strategy (DLS) was then considered to optimize the locations and sizes while maintaining a balance between the exploration and exploitation phases. Three IEEE RDNs were used to simulate various EV load increase scenarios as well as typical loading situations. According to a comparison with the literature, the IPFA produced global optimum results, and the proposed CBs allocation approach demonstrated enhanced performance in RDNs under all scenarios of EV load growth.

**Keywords:** Capacitor banks allocation, Electric vehicle load, Improved flower pollination algorithm, Net-cost optimization, Radial distribution network, VAr compensation, Voltage stability index.

## 1 Introduction

Radial distribution networks (RDNs) suffer from high distribution losses, low voltage profiles, low reliability, reduced stability margins, and high x/r ratios owing to their radial configuration [1]. This situation could deteriorate further for emerging high EV load growth scenarios worldwide, resulting in voltage collapse or power system blackouts, as seen in many power systems over the last two decades [2]. In this scenario, optimizing the RDN performance becomes critical from both technical and economic standpoints. The optimal integration of

[1]Department of Electrical and Electronics Engineering, School of Engineering and Technology, CHRIST (Deemed to be University), Bangalore – 560074, Karnataka, India;
E-mail: varaprasad.janamala@christuniversity.in

capacitor banks (CBs) [3], distribution generation (DGs) [4], and network reconfiguration [5] are some of the approaches employed in the literature to improve the performance of RDNs. Among these approaches, utilities commonly integrate switched and fixed CBs to ensure an adequate voltage profile across the network. However, in the literature, the best location identification (discrete variables) and proper size evaluation (continuous variables) have been viewed as multi-objective optimization problems with multiple variables and multiple equal and unequal constraints that can be solved effectively using various heuristic approaches [6].

In [7], the optimal locations and sizes were determined using the gravitational search algorithm (GSA) while considering net savings maximization. Suitable locations were selected using loss sensitivity factors (LSFs) and norm voltage profiles. In [8], the modified artificial bee colony (MABC) method was used to solve the CBs allocation problem, and the energy loss cost and overall capacitor cost were optimized. Clonal selection algorithm (CSA) is used to solve the CBs allocation problem with the goals of loss minimization and voltage profile enhancement [9]. In [10, 11], the flower pollination algorithm (FPA) was used to solve the CBs allocation problem to maximize net savings. To address the allocation of CBs and DGs for techno-economic-environmental benefits, the water cycle algorithm (WCA) was used [12]. In [13], potential locations were identified using LSFs and voltage stability indices (VSIs), and the optimal positions and sizes of CBs under various loading conditions were then determined using the improved bacterial foraging optimization algorithm (IBFOA). In [14], grey wolf (GWO), dragonfly (DFO), and moth-flame (MFO) optimizers were used to allocate CBs to minimize costs and reduce losses. The salp swarm algorithm (SSA) was employed in [15] to optimize the techno-economic-environmental difficulties when installing CBs and DGs in an RDN. In [16], an improved stochastic fractal search (ISFS) combining quasi-opposition-based learning (QOBL) and chaotic local search (CLS) strategies was used to optimize the energy loss cost, capacitor operation, and installation expenses. In [17], the polar bear optimization algorithm (PBOA) is adapted for CBs allocation to optimize techno-economic benefits. To solve CBs/DGs, the honey badger algorithm (HBA) is presented, considering the minimization of energy loss, total VSI, and voltage deviation index (VDI) [18]. In [19], a whale optimization algorithm (WOA) was proposed to solve CBs for loss reduction and operating cost minimization by maintaining a better voltage profile. In [20], LSFs based weak candidate buses were identified, and the mine blast algorithm (MBA) was employed to determine the optimal locations and sizes of CBs considering techno-economic objectives. In [21], LSFs and VSIs were used to determine the candidate locations for CBs, and the bacterial foraging optimization algorithm (BFOA) was used for optimal locations and sizes towards loss reduction under different loading conditions.

These studies show that proper CB placement in RDNs can guarantee improved performance from technical and financial standpoints. Many of these problems are solved in two steps. Through the use of sensitivity analysis tools such as LSFs and VSIs, the prospective candidate locations are identified in stage 1. Meta-heuristics are employed in Stage 2 to choose the best locations and sizes for CBs. However, only a limited number of studies have used algorithms to directly determine the locations and sizes of CBs. According to the no-free-lunch (NFL) theorem [22], there is no single algorithm capable of solving all types of complex optimization problems. Consequently, researchers are constantly developing new algorithms to introduce and adapt, as well as ways to improve existing ones. The flower pollination algorithm (FPA) [23] is a simple and effective method introduced by Xin-She Yang in 2012, which uses the pollination process of flowers. Since its introduction, the FPA has attracted the attention of various researchers for different optimization problems. Despite being simple and easy to implement, the basic FPA has local minima when handling complex and high-dimensional optimization problems. FPA has a plethora of advanced variants to improve its performance [24]. To prevent local optima, improvements to the global search's double-direction learning strategy (DLS), the local search's greedy strategy, and the dynamic switching probability strategies of global and local search were proposed in [25] for developing an improved flower pollination algorithm (IFPA).

In this study, the problem of the optimal allocation of CBs (OACP) in RDNs is reframed in light of the emerging EV load penetration, which has not been considered in the literature. In addition to using VSIs to determine weak candidate locations as a predefined search space in the first stage, the current work differs from previous studies on OACB that used PLI-FPA [10] and FPA [11]. In the second stage, the IFPA deduces the ideal sites and their sizes to minimize the multi-objective function formulated for techno-economic goals. Simulations were performed on standard IEEE 33-, 69-, and 85-bus RDNs and compared with the literature. Studies have also been extended to different EV load penetration levels, and the impact of optimal CBs at appropriate locations has been realized in terms of reduced losses, improved voltage profile, enhanced voltage stability, and increased net savings.

## 2 Modeling of Electric Vehicle Load Growth

Knowing the load increase of a specific load type is crucial for the planning and control operations of the system operator. Here, it is expected that all EV types are connected to utilities via an AC/DC converter or charging connector. Because batteries are the primary source of electricity for EVs, voltage-dependent load modeling was used to simulate the accompanying load [26]. After the EV

integration, the active and reactive power demands at bus *n* are expressed as follows:

$$P_{d(n)}^{t} = P_{L(n)}^{0} \times \left( \frac{V_{(n)}^{t}}{V_{(n)}^{0}} \right)^{\alpha} + \left\{ P_{ev(n)}^{0} \times \left( \frac{V_{(n)}^{t}}{V_{(n)}^{0}} \right)^{\alpha_{ev}} \right\}, \tag{1}$$

$$Q_{d(n)}^{t} = Q_{L(n)}^{0} \times \left( \frac{V_{(n)}^{t}}{V_{(n)}^{0}} \right)^{\beta} + \left\{ Q_{ev(n)}^{0} \times \left( \frac{V_{(n)}^{t}}{V_{(n)}^{0}} \right)^{\beta_{ev}} \right\}, \tag{2}$$

where $P^{0}_{L(n)}$ and $Q^{0}_{L(n)}$ are the nominal real and reactive power loads at bus *n*, respectively; $P^{t}_{L(n)}$ and $Q^{t}_{L(n)}$ are the modified real and reactive powers at time *t*, respectively; $P^{0}_{d(n)}$ and $Q^{0}_{d(n)}$ are the real and reactive power loads at location *n* after integration of the EV load, respectively; $P^{0}_{ev(n)}$ is the additional load owing to the integration of EVs at that location; $V^{0}_{(n)}$ and $V^{t}_{(n)}$ are the voltage magnitudes of bus-*n* at the nominal and specified times, respectively; α and β are the exponents for real and reactive powers, respectively; and $\alpha_{ev}$ and $\beta_{ev}$ are the exponents of EV's real and reactive power loads, respectively.

The additional real and reactive power loads at bus *n* owing to EVs are given by

$$P_{ev(n)}^{0} = P_{L(n)}^{0} \left( 1 + \frac{a}{100} \right)^{b}, \tag{3}$$

$$Q_{ev(n)}^{0} = P_{ev(n)}^{0} \times \tan\left( \phi_{n(c)} \right), \tag{4}$$

where *a* is the load growth rate, *b* is the number of years, and $\phi_{n(c)}$ is the operating power factor (p.f.) angle of the AC/DC converter.

## 3 Load Flow Solution and Voltage Stability Index

The examination of load flow is a crucial first step in determining the functioning of a distribution system. Among the different methods that are already available [27], the backward/forward sweep (BFS) method suggested in [28] is described here and used for the development of the VSI [29].

### 3.1 Backward/forward sweep load flow solution

By considering a typical two-bus test system, as shown in Fig. 1, the mathematical relations employed in the backward/forward sweep (BFS) load flow method [28] are presented. The branch impedance between buses *m* and *n* and the complex power at bus *n* are considered to be $Z_{(pq)} = r_{(pq)} + jx_{(pq)}$ and $S_{(q)} = P_{(q)} + jQ_{(q)}$, respectively.

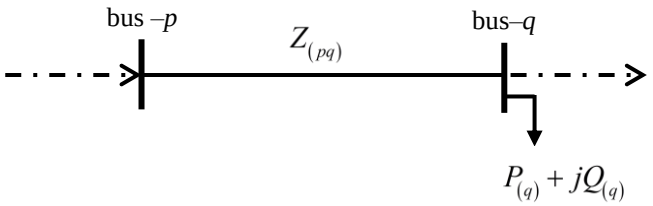


**Fig. 1 –** *Typical two-bus test system.*

The branch current is given by,

$$I_{(pq)} = I_{(q)} = \left(S_{(q)}/V_{(q)}\right)^{*}, \tag{5}$$

$$\Rightarrow \quad \frac{\left|V_{(p)}\right|\angle\delta_{(p)} - \left|V_{(q)}\right|\angle\delta_{(q)}}{r_{(pq)} + jx_{(pq)}} = \frac{P_{(q)} - jQ_{(q)}}{\left|V_{(q)}\right|\angle -\delta_{(q)}}, \tag{6}$$

$$\Rightarrow \quad \left[\left|V_{(p)}\right|\angle\delta_{(p)} - \left|V_{(q)}\right|\angle\delta_{(q)}\right]\left|V_{(q)}\right|\angle -\delta_{(q)} = \left(P_{(q)} - jQ_{(q)}\right)\left(r_{(pq)} + jx_{(pq)}\right), \tag{7}$$

$$\Rightarrow \quad \left[\left|V_{(p)}\right|\left|V_{(q)}\right|\angle\left(\delta_{(p)} - \delta_{(q)}\right) - \left|V_{(q)}\right|^{2}\right] = \left(P_{(q)} - jQ_{(q)}\right)\left(r_{(pq)} + jx_{(pq)}\right). \tag{8}$$

By separating real and imaginary parts, we have,

$$\left|V_{(p)}\right|\left|V_{(q)}\right|\cos\left(\delta_{(pq)}\right) = P_{(q)}r_{(pq)} + Q_{(q)}x_{(pq)} + \left|V_{(q)}\right|^{2}, \tag{9}$$

$$\left|V_{(p)}\right|\left|V_{(q)}\right|\sin\left(\delta_{(pq)}\right) = P_{(q)}x_{(pq)} - Q_{(q)}r_{(pq)}. \tag{10}$$

Squaring and adding (9) and (10) and simplifying, we obtain,

$$\left|V_{(q)}\right|^{4} - k_1\left|V_{(q)}\right|^{2} + k_2 = 0, \tag{11}$$

where $k_1$ and $k_2$ are given by (12) and (13):

$$k_1 = \left|V_{(p)}\right|^{2} - 2P_{(q)}r_{(pq)} - 2Q_{(q)}x_{(pq)}, \tag{12}$$

$$k_2 = \left(P_{(q)}^{2} + Q_{(q)}^{2}\right)\left(r_{(pq)}^{2} + x_{(pq)}^{2}\right). \tag{13}$$

Based on the feasible solution of (11), the voltage magnitude of bus-*q* and its phase angles are given by (14) and (15):

$$\left|V_{(q)}\right| = \left[\frac{1}{2}k_1 + \left(k_1^{2} - 4k_2\right)^{\frac{1}{2}}\right]^{\frac{1}{2}}, \tag{14}$$

$$\delta_{(q)} = \delta_{(p)} - \tan^{-1}\left[\frac{\left(P_{(q)}x_{(pq)} - Q_{(q)}r_{(pq)}\right)}{\left|V_{(q)}\right|^2 + P_{(q)}r_{(pq)} + Q_{(q)}x_{(pq)}}\right]. \quad (15)$$

Using the voltage profile, the real and reactive powers of a branch and, consequently, the total network losses can be determined using the following:

$$P_{loss(pq)} = r_{(pq)}\left(\frac{P_{(q)}^2 + Q_{(q)}^2}{\left|V_{(q)}\right|^2}\right), \quad (16)$$

$$Q_{loss(pq)} = x_{(pq)}\left(\frac{P_{(q)}^2 + Q_{(q)}^2}{\left|V_{(q)}\right|^2}\right), \quad (17)$$

$$P_{T,loss} = \sum_{pq=1}^{nbr} P_{loss(pq)}\ , \quad (18)$$

$$Q_{T,loss} = \sum_{pq=1}^{nbr} Q_{loss(pq)}\ . \quad (19)$$

Initially, $P_{loss(pq)}$ and $Q_{loss(pq)}$ for all the branches were set to zero. By knowing bus-*p* voltage magnitude and its load angle ($|V_{(p)}| = 1.0$ p.u. & $\delta_{(p)} = 0$), the initial effective powers $P_{(q)}$ and $Q_{(q)}$ are determined by summing all the loads beyond bus-*q* plus local load of bus-*q*. Subsequently, the real and reactive power losses of branch *pq* are determined using (16) and (17). By proceeding for all branches, the total power loss of the system can be determined using (18) and (19). This stage completes one iteration. By updating the bus injections $P_{(q)} = P_{(q)} + P_{loss(pq)}$ and $Q_{(q)} = Q_{(q)} + Q_{loss(pq)}$, the procedure continues until the convergence criterion $\varepsilon = \max\{(|V^{t+1}_{(p)}| - (|V^{t}_{(p)}| \leq 10^{-5}\}$ (i.e., the maximum change in voltage magnitude between two consecutive iterations of all buses).

### 3.2 Voltage stability index

As specified in [29], the VSI of a branch's receiving-end bus can be computed using the sending-end bus voltage, real and reactive power loads, and resistance and reactance.

$$VSI_{(q)} = \left[\left|V_{(p)}\right|^4 - 4\left(P_{(q)}x_{(pq)} - Q_{(q)}r_{(pq)}\right) - 4\left(P_{(q)}r_{(pq)} + Q_{(q)}x_{(pq)}\right)\left|V_{(p)}\right|^2\right]. \quad (20)$$

Stable operation requires a $VSI_{(q)}$ above 0. The smallest VSI value among all the buses is considered to be the system stability. Thus, using low-VSI buses for CB integration can enhance overall voltage stability. By sorting all buses according to their VSI values, top-ten locations are used as preferred locations to reduce the search space and thus ensure effective convergence.

### 3.3 Net-savings calculation

The net savings can be realized because CBs integration is determined using savings owing to a reduction in distribution losses and cost of CBs installation:

$$NS_{cb} = k_p \left[ P_{T,loss(0)} - P_{T,loss(c)} \right] - \sum_{i=1}^{ncb} k_{c(i)} Q_{cap(i)}, \tag{21}$$

where $NS_{cb}$ is the net savings due to CBs installation, and $P_{T,loss(0)}$ and $P_{T,loss(t)}$ are the total real power losses before and after installation of CBs in the distribution system, which can be determined using (18), $k_p$ is the cost of power in \$/kW; $k_c$ is the cost of CB in \$/kVAr, $Q_{cap(i)}$ is the size of the CB in kVAr at bus *i*, and *ncb* is the number of CB locations.

## 4 Problem Formulation

The major goal of this research is to minimize the total real power losses and, as a result, to maximize net savings, improve the voltage profile, and enhance voltage stability.

$$OF = \min\left( P_{T,loss} \right). \tag{22}$$

The OF is limited by constraints such as (i) supply-demand balance, (ii) voltage limits, and (iii) reactive power compensation limits, which are given by

$$P_{eff(sub)} + jQ_{eff(sub)} = \left( \sum_{i=1}^{n} P_{d(i)} + P_{T,loss(c)} \right) + j\left( \sum_{i=1}^{n} Q_{d(i)} + Q_{T,loss(c)} \right), \tag{23}$$

$$\left| V_{(i)}^{\min} \right| \le \left| V_{(i)} \right| \le \left| V_{(i)}^{\max} \right|, \tag{24}$$

$$\frac{\sum_{i=1}^{ncb} Q_{cap(i)}}{\sum_{i=1}^{n} Q_{d(i)}} \le 1, \tag{25}$$

where $P_{eff(sub)}$ and $Q_{eff(sub)}$ are the real and reactive power demands on the substation, respectively; $P_{d(i)}$ and $Q_{d(i)}$ are the real and reactive power loads at bus *i*, respectively; *n* is the number of buses in the network; and $|V_{(i)}|$, $|V^{min}_{(i)}|$, and $|V^{max}_{(i)}|$ are the voltage magnitude of bus *i*, and its minimum and maximum limits, respectively.

## 5 Modeling of Improved Flower Pollination Algorithm

In the last two decades, nature-inspired metaheuristic optimization algorithms have gained popularity. This technique improves random solutions generated by their stochastic nature. The second stage replicates the nature of the element until the stopping criterion is reached. Yang et al.'s 2012 flower

pollination algorithm (FPA) is simple, straightforward to implement, and efficient [23].

### 5.1 Basic flower pollination algorithm

This section describes the main pollinator features and FPA components based on the natural relationship between flowering plants and pollinators. Insects, butterflies, and birds are variables, whereas pollen/flowers are solution vectors. Similar vector solutions are referred to as floral consistency solutions. Biological pollination symbolizes global searches and abiotic pollination symbolizes local searches. The initial random solution vector can be corrected via Lévy flight and fresh flowers can be represented as new solution vectors in each iteration. The optimal answer to the end-of-maximum iterations is flower reproduction.

The biotic pollination for global search or rule 1 is depicted as follows:

$$v_i^{k+1} = v_i^k + \gamma L\left(v_{best}^k - v_i^k\right), \tag{26}$$

where $v^k_{best}$ is the best pollen discovered among all pollens at iteration $k$, $L$ is the step size, essentially used to denote the strength of pollination, and $v^k_i$ is pollen $i$ or solution vector $i$ at iteration $k$. This can be acquired by applying the Lévy flight described in (27):

$$L \sim \frac{\lambda\Gamma(\lambda)\sin(\pi\lambda/2)}{\pi}\frac{1}{s^{1+\lambda}}, \quad (s \geq 0), \tag{27}$$

where $\Gamma(\lambda)$ denotes the standard gamma function; this distribution is valid for steps $s > 0$, $\lambda = 1.5$, and

$$s = U/|V|^{1/\lambda}.$$

Here, $V$ is a random number with a standard normal distribution and $U$ is a Gaussian distribution with variance $\delta^2$.

Similarly, abiotic pollination or *rule 2* is represented as:

$$v_i^{k+1} = v_i^k + \varepsilon\left(v_l^k - v_m^k\right), \tag{28}$$

where $v^k_l$ and $v^k_m$ are the pollen from different flowers of the same plant type at iteration $k$, and $\varepsilon$ is a random distribution in [0, 1].

In this phase, the distinction between exploration and local search spaces is made. Following testing by Yang, the switching parameter p defined the type of pollination for each population/flower, and its best value was 0.8. Local pollination is performed and gives the algorithm exploitation property if the random number generated for $\varepsilon$ is larger than $p$; otherwise, global pollination is followed, giving the algorithm exploration property. This procedure continues

until the convergence condition, that is, the maximum number of iterations, is satisfied.

### 5.2 Modifications for IFPA

The modifications proposed in [25] are discussed herein for the development of an improved flower pollination algorithm (IFPA). The dynamic switching probability for mapping the exploration and exploitation phases is given by

$$p_a^k = p_{a,\min} + \exp\left(-10 \times \frac{t}{k_{\max}}\right)\left(p_{a,\max} - p_{a,\min}\right). \tag{29}$$

The search for global pollinators, determined using (26), and a greedy solution, as defined by (30).

$$v_i^{'k+1} = v_i^k + \gamma L\left(v_m^k - v_i^k\right). \tag{30}$$

The search for the local best is determined using (31) and (32),

$$v_i^{k+1} = v_i^k + \varepsilon\left(v_j^k - v_l^k\right) + S, \tag{31}$$

$$S = \alpha\left\{\omega\left(v_{best}^k - v_i^k\right) + (1-\omega)\left(v_{best}^{k-1} - v_i^k\right)\right\}, \tag{32}$$

where: $v^k_{best}$ and $v^{k-1}_{best}$ are the best solutions of $k$ and ($k$-1) iterations, respectively; $\omega$ is a weighting coefficient for obtaining the proportion of ($v^k_{best} - v^k_i$) and ($v^{k-1}_{best} - v^k_i$).

$\alpha \in (0,1)$ is the scaling factor for adjusting the step size.

The complete procedure of the IFPA as a flow chart for solving the CBs allocation problem is shown in Fig. 2.

## 6 Results and Discussions

The simulations were executed using a PC with a 2.30 GHz Intel Core i5-2410M CPU, 64-bit operating system, and 4 GB of RAM in a MATLAB environment on IEEE 33-, 69-, and 85-bus RDNs. Section 6.1 discusses the network performance without CBs and EVs. Section 6.2 examines and evaluates the IFPA-based CB allocation. Section 6.3 examines the impact of increasing the EV load without CBs. Section 6.4 optimizes CB distribution for each EV demand scenario. For all test systems, 168 $/kWh/year was chosen as the cost of genuine power loss [7], and the costs and realistically available capacitor sizes in kVAr were taken from [19]. It is assumed that the switching probability has minimum and maximum limits of 0.2 and 0.8, respectively [25]. The maximum number of iterations was 50 and the population size was assumed to be 20.

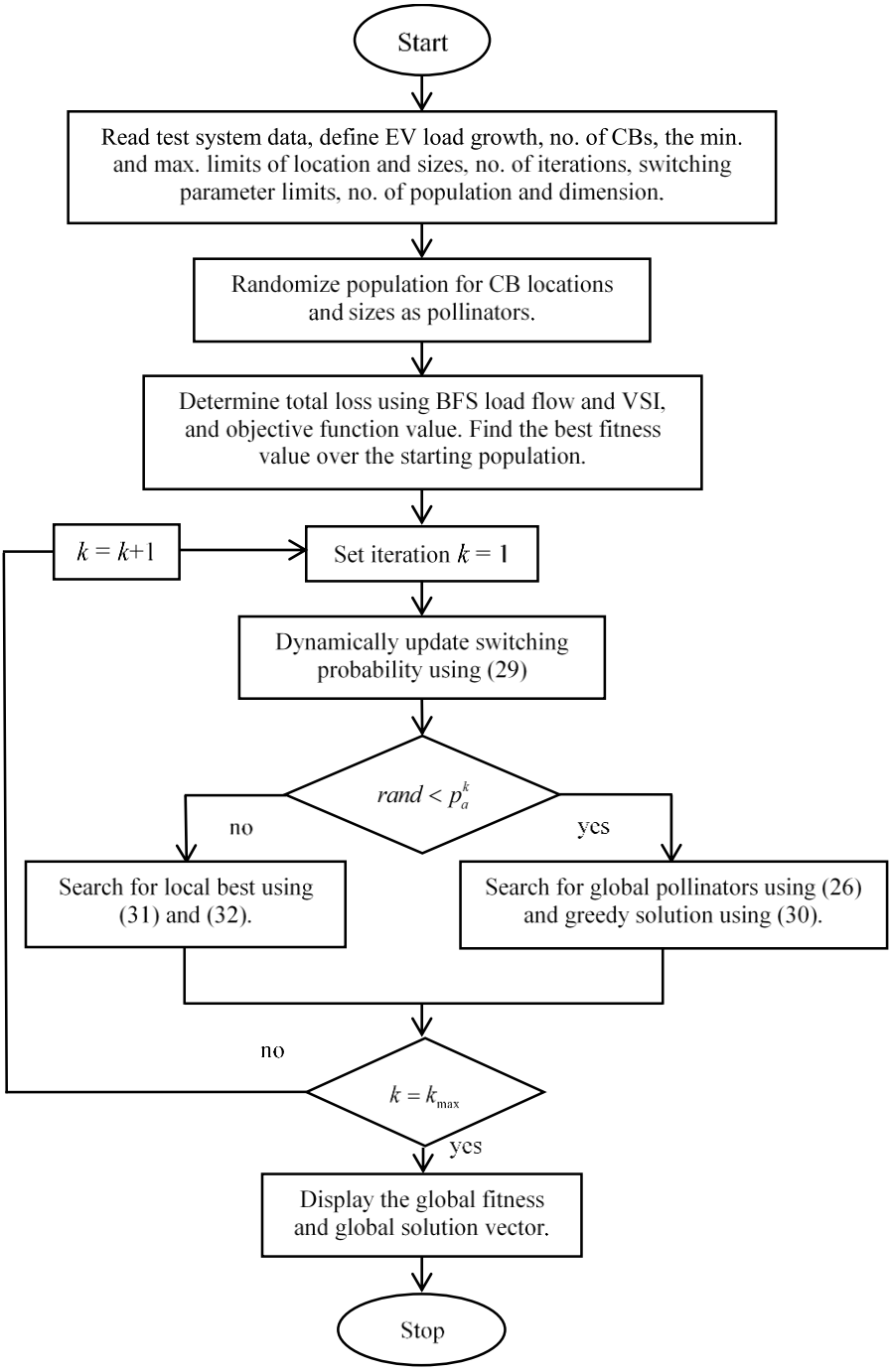


**Fig. 2** – *Flowchart for IFPA while solving CBs allocation problem.*

### 6.1 Network performance for base case

In this case, the OACP is handled without considering the EV load growth and is compared with the results obtained via IFPA with existing literature. The data of the IEEE 33-, 69-, and 85-bus test systems were taken from [30, 31], and [19], respectively. The performance of the three uncompensation test systems is listed in **Table 1**.

The IEEE 33-bus RDN has a total real and reactive power consumption of 3715 kW and 2300 kVAr, respectively, and comprises 33 buses connected by 32 branches. When performing load flow [23], base values of 100 MVA and 12.66 kV are used. The uncompensated system had a reactive power of 135.1409 kVAr and a real power loss of 202.6771 kW. At bus-18, it has the lowest voltage of 0.9131 p.u. With a value of 0.6575 for the VSI calculated in accordance with [24], the system is considered to have a low voltage stability. The total running cost in this instance is 34049.75 $.

The IEEE 69-bus RDN, which consists of 69 buses connected by 68 branches, has total real and reactive power consumption of 3802.1 kW and 2694.7 kVAr, respectively. Base values of 100 MVA and 12.66 kV were used to perform the load flow. The uncompensated system had a reactive power of 102.1648 kVAr and an actual power loss of 225 kW. Its lowest voltage, 0.9092 p.u., was at bus-65. The system was deemed to have low voltage stability when the VSI, calculated in accordance with [24], had a value of 0.55. In this case, the total running expense is 37800.11 $.

The total actual and reactive power consumption of the IEEE 85-bus RDN, which comprises 85 buses connected by 84 branches, is 2570.28 kW and 2622.08 kVAr, respectively. To perform load flow, the default values of 100 MVA and 11 kV were employed. The uncompensated system has an actual power loss of 316.1175 kW and reactive power of 198.6021 kVAr. At bus-54, it has a voltage of 0.8713 p.u. If VSI, as determined by [24], has a value of 0.5664, the system is said to have low voltage stability. The total running cost in this instance is 53107.74 $.

**Table 1**
*Performance of uncompensation networks.*

| Parameter | Test System | | |
|---|---|---|---|
| | 33-bus | 69-bus | 85-bus |
| $P_{load}$ (kW) | 3715 | 3802.10 | 2570.28 |
| $Q_{load}$ (kVAr) | 2300 | 2694.70 | 2622.08 |
| $P_{loss}$ (kW) | 202.6771 | 225.0007 | 316.1175 |
| $Q_{loss}$ (kVAr) | 135.141 | 102.1648 | 198.6021 |
| $V_{min}$ (p.u.)/ bus # | 0.9131/ 18 | 0.9092/ 65 | 0.8713/ 54 |
| VSI | 0.6575 | 0.55 | 0.5664 |
| $P_{loss}$ Cost ($)$_B$ | 34049.75 | 37800.11 | 53107.74 |

### 6.2 Network performance for optimal CBs allocation

In this case, the network performance is optimized for base-case loading conditions by optimally integrating the three CBs. Thus, the search space dimension is six (i.e., three for locations and three for sizes). The best results obtained from over 50 independent run simulations of the IPFA are listed in **Table 2**. The performance of the IPFA is quantified in terms of the median and standard deviation (std.) and the computational time is also provided. On the other hand, the comparisons with literature are given in **Tables 3, 4,** and **5** for IEEE 33-, 69-, and 85-bus RDNs, respectively.

**Table 2**
*Performance of compensation networks.*

| Parameter | Compensation by IFPA | | |
|---|---|---|---|
| | 33-bus | 69-bus | 85-bus |
| CB sizes in kVAr/bus# | 300/14<br>600/24<br>1050/30 | 300/52<br>1200/61<br>300/21 | 600/48<br>1350/8<br>450/68 |
| Compensation (%) | 84.78 | 66.8 | 91.53 |
| CB Cost ($/kVAr)$_A$ | 476.4 | 414 | 525.3 |
| $P_{loss}$ (kW) | 132.4256 | 145.9872 | 151.8377 |
| $Q_{loss}$ (kVAr) | 88.5522 | 67.9926 | 94.3399 |
| $V_{min}$ (p.u.)/ bus # | 0.9368/18 | 0.9307/ 65 | 0.925/54 |
| VSI | 0.7501 | 0.7152 | 0.721 |
| $P_{loss}$ Cost ($)$_B$ | 22247.51 | 24525.86 | 25508.73 |
| Total Cost ($)$_{A+B}$ | 22723.91 | 24939.86 | 26034.03 |
| Net Savings (%) | 33.26 | 34.02 | 50.981 |
| $P_{loss}$ Reduction (%) | 34.66 | 35.12 | 51.971 |
| Best | 132.4256 | 145.9872 | 151.8377 |
| Median | 132.445 | 146.491 | 152.132 |
| Std. | 3.571 | 4.764 | 6.265 |
| Average Time (sec) | 1.5417 | 4.0826 | 5.1747 |

The best locations in the IEEE 33-bus are 14, 24, and 30, and the sizes in kVAr are 300, 600, and 1050, respectively. By having approximately 84.78 % VAr compensation by these CBs, the network's real and reactive power losses are reduced to 132.4256 kW and 88.5522 kVAr, respectively. The lowest voltage was 0.9368 p.u. at bus-18, and the overall VSI was determined to be 0.7501. In comparison to the base case, the real power losses are decreased by 34.66 %, and the overall net-savings were 33.26 %. As shown in **Table 3**, the results obtained using IPFA are better than those reported in the literature for GSA [7], IBFOA [13], PBOA [17], SSA [15], MFO [14], GWO [14], DFO [14], PSO [14], FPA [11], and CSA [9]. In contrast to these works with fixed CBs (discrete), further improvement can be observed with switching CBs (continuous), as determined in the WCA [12].

**Table 3**
*Comparison of IPFA results in IEEE 33-bus.*

| Method | CB size in kVAr/ bus # | $P_{Loss}$ (kW) | VSI |
|---|---|---|---|
| Base | – | 202.6771 | 0.6575 |
| GSA [7] | 350/26, 450/13, 800/15 | 187.0814 | 0.703 |
| IBFOA [13] | 695/18, 525/25, 850/30 | 147.892 | 0.767 |
| PBOA [17] | 318/6, 294/13, 709/29 | 139.722 | 0.726 |
| SSA [15] | 450/10, 450/23, 1050/29 | 135.816 | 0.758 |
| MFO, GWO, DFO, PSO [14] | 450/8, 300/13, 900/30 | 134.149 | 0.759 |
| FPA [11] | 900/30, 450/13, 450/24 | 132.982 | 0.756 |
| CSA [9] | 900/30, 400/12, 550/24 | 132.867 | 0.741 |
| WCA [12] | 397.3/14, 451.1/24, 1000/30 | 132.429 | 0.760 |
| **Proposed** | **450/14, 450/24, 1050/30** | **132.4256** | **0.7501** |

**Table 4**
*Comparison of IPFA results in IEEE 69-bus.*

| Method | CB size in kVAr/ bus # | $P_{Loss}$ (kW) | VSI |
|---|---|---|---|
| Base | – | 225 | 0.55 |
| GSA [7] | 150/26, 150/13, 1050/15 | 230.027 | 0.562 |
| HBA [18] | 413.14/11, 230.7/21, 232.41/61 | 185.911 | 0.591 |
| IBFOA [13] | 432/65, 420/60, 828/10 | 155.77 | 0.593 |
| SSA [15] | 300/17, 1200/60, 300/10 | 150.529 | 0.605 |
| ISFSA [16] | 250/20, 1150/61 | 147.762 | 0.709 |
| FPA [10] | 1250/61, 250/24 | 147.195 | 0.714 |
| PSO [14] | 450/17, 1350/61 | 147.023 | 0.755 |
| MFO, GWO, DFO [14] | 300/17, 1350/61 | 146.702 | 0.754 |
| CSA [9] | 300/64, 300/23, 950/61 | 146.554 | 0.706 |
| **Proposed** | **300/52, 1200/61, 300/21** | **145.9872** | **0.7152** |

**Table 5**
*Comparison of IPFA results in IEEE 85-bus.*

| Method | CB size in kVAr/ bus # | $P_{Loss}$ (kW) | VSI |
|---|---|---|---|
| Base | | 316.1353 | 0.567 |
| FPA [11] | 1200/8, 600/72, 600/36 | 189.461 | 0.667 |
| GSA [7] | 150/8, 150/12, 350/29, 450/36, 450/68, 1050/83 | 181.711 | 0.724 |
| MABC [8] | 600/8, 600/58, 150/7, 900/27 | 163.457 | 0.686 |
| PBOA [17] | 492/11, 456/30, 357/47, 350/62, 375/67 | 153.759 | 0.697 |
| BFOA [21] | 840/9,660/34, 650/60 | 152.903 | 0.703 |
| MBA [20] | 800/8, 300/27, 400/34, 400/58, 300/64 | 151.892 | 0.700 |
| **Proposed** | **600/48, 1350/8, 450/68** | **151.8377** | **0.721** |

The optimal IEEE 69-bus locations were 52, 61, and 21, and the optimal sizes in kVAr were 300, 1200, and 300, respectively. The network's actual and reactive power losses are decreased to 145.9872 kW and 67.9926 kVAr, respectively, by these CBs compensating for approximately 66.8 % of VAr. The overall VSI was calculated as 0.7152, and the lowest voltage was 0.9307 p.u. at bus-65. real power losses were reduced by 35.12 % as compared to the base case, while overall net

savings were 34.02 %. As shown in **Table 4**, the results from IPFA are superior to those from the literature works GSA [7], HBA [18], IBFOA [13], SSA [15], ISFSA [16], FPA [10], PSO [14], MFO [14], GWO [14], DFO [14], and CSA [9].

The ideal sites for an IEEE 85-bus system are 48, 8, and 68, while the ideal sizes are 600, 1350, and 450 kVAr. These CBs compensate for approximately 91.53 percent of VAr, lowering the actual and reactive power losses of the network to 151.8377 kW and 94.3399 kVAr, respectively. The lowest voltage was 0.925 p.u. at bus-54, and the calculated total VSI was 0.721. In comparison to the base case, real power losses are decreased by 51.971 %, and overall net savings are decreased by 50.981 %. As shown in **Table 5**, the IPFA results are better than those from the literature: FPA [11], GSA [7], MABC [8], PBOA [17], BFOA [21], and MBA [20].

The convergence characteristics of the IPFA for producing the best results given in **Table 2** are shown in Fig. 3 for IEEE 33-, 69-, and 85-bus RDNs, respectively.

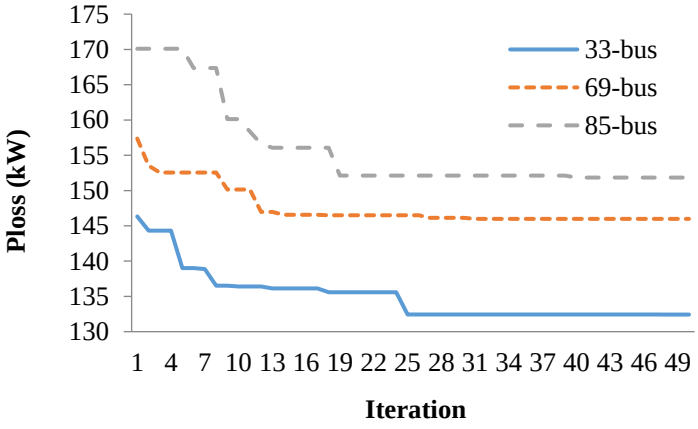


**Fig. 3** – *Convergence characteristics of IFPA for best results.*

### 6.3 Network performance with EV load penetration

The performance of the system for different annual load growth scenarios is presented in **Tables 6**, **7**, and **8** for the IEEE 33-, 69-, and 85-bus RDNs, respectively. The case study reveals that the performance of the networks decreases significantly as the EV load penetration increases. Both the real and reactive power losses are increased, the voltage profile decreases, and correspondingly, the voltage stability margin is significantly reduced. In addition, the real power loss cost increases owing to the increment in the losses.

**Table 6**
*Performance of IEEE 33-bus with EV load before CBs allocation.*

| Parameter | Annual EV load growth (%) | | | | |
|---|---|---|---|---|---|
| | 10 | 20 | 30 | 40 | 50 |
| $P_{load}$ (kW) | 4040.31 | 4360.13 | 4674.78 | 4984.54 | 5289.67 |
| $Q_{load}$ (kVAr) | 2467.25 | 2625.96 | 2776.63 | 2919.62 | 3055.33 |
| $P_{loss}$ (kW) | 236.7125 | 272.6538 | 310.3766 | 349.8189 | 390.8679 |
| $Q_{loss}$ (kVAr) | 157.7063 | 181.5201 | 206.4815 | 232.5833 | 259.7336 |
| $V_{min}$ (p.u.) | 0.9058 | 0.8987 | 0.8917 | 0.8850 | 0.8784 |
| VSI | 0.6721 | 0.6514 | 0.6316 | 0.6128 | 0.5948 |
| $P_{loss}$ Cost ($) | 39767.7 | 45805.83 | 52143.28 | 58769.58 | 65665.81 |

**Table 7**
*Performance of IEEE 69-bus with EV load before CBs allocation.*

| Parameter | Annual EV load growth (%) | | | | |
|---|---|---|---|---|---|
| | 10 | 20 | 30 | 40 | 50 |
| $P_{load}$ (kW) | 4128.46 | 4449.95 | 4766.26 | 5077.74 | 5384.72 |
| $Q_{load}$ (kVAr) | 2875.37 | 3050.17 | 3218.45 | 3380.62 | 3536.96 |
| $P_{loss}$ (kW) | 261.0476 | 298.8965 | 338.3136 | 379.1960 | 421.4758 |
| $Q_{loss}$ (kVAr) | 118.7659 | 136.2485 | 154.5083 | 173.4561 | 193.1494 |
| $V_{min}$ (p.u.) | 0.9021 | 0.8951 | 0.8884 | 0.8817 | 0.8753 |
| VSI | 0.6613 | 0.6412 | 0.6221 | 0.6039 | 0.5864 |
| $P_{loss}$ Cost ($) | 43856 | 50214.61 | 56836.69 | 63704.94 | 70807.93 |

**Table 8**
*Performance of IEEE 85-bus with EV load before CBs allocation.*

| Parameter | Annual EV load growth (%) | | | | |
|---|---|---|---|---|---|
| | 10 | 20 | 30 | 40 | 50 |
| $P_{load}$ (kW) | 2769.130 | 2960.550 | 3145.070 | 3323.140 | 3495.180 |
| $Q_{load}$ (kVAr) | 2798.450 | 2964.870 | 3122.220 | 3271.260 | 3412.660 |
| $P_{loss}$ (kW) | 366.860 | 419.530 | 473.700 | 529.160 | 585.730 |
| $Q_{loss}$ (kVAr) | 230.540 | 263.700 | 297.820 | 332.760 | 368.420 |
| $V_{min}$ (p.u.) | 0.8616 | 0.8519 | 0.8425 | 0.8334 | 0.8246 |
| VSI | 0.5511 | 0.5266 | 0.5038 | 0.4824 | 0.4624 |
| $P_{loss}$ Cost ($) | 431807 | 465214 | 497372 | 528372 | 558288 |

### 6.4 Network performance with EV load penetration and optimal CBs

In this case study, the performance of each network is proposed to be enhanced by optimally integrating the CBs under each EV load growth condition. Because the EV load is more stochastic in nature, a dynamic VAr support was used in this case study. In this connection, this case study is performed with discrete CB sizes with an increment of 5 kVAr. The cost for unavailable CB sizes in [19] was determined using the shape-preserving interpolation curve-fitting method in MATLAB. The performance of the networks with IFPA-based CBs

integration is presented in **Tables 9**, **10**, and **11** for IEEE 33-, 69-, and 85-bus RDNs, respectively.

A better understanding of the effects of CB allocation under the scenario of increasing EV load is provided by a comparison of $P_{loss}$ and VSI for all three test systems, as shown in **Fig. 4**.

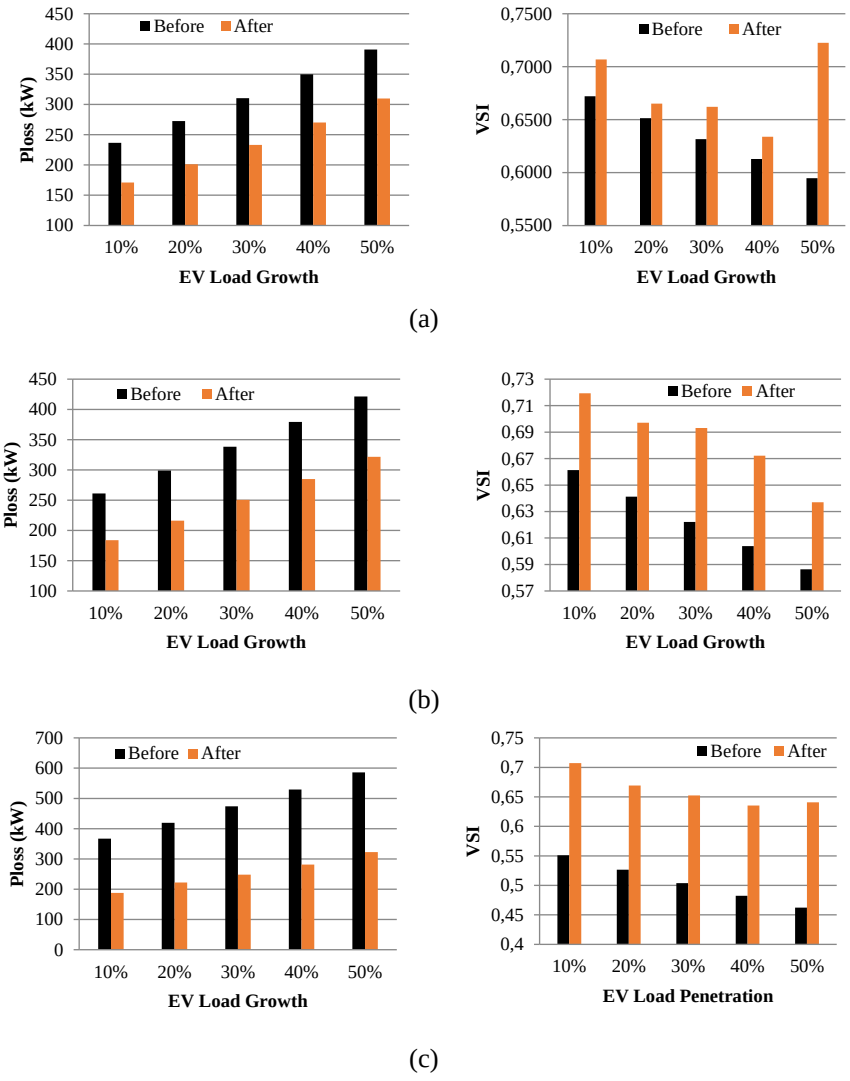


**Fig. 4** – *Comparison of Ploss and VSI before and after CBs under each EV load growth:* (a) *IEEE 33-bus RDN;* (b) *IEEE 69-bus RDN;* (c) *IEEE 85-bus RDN.*

According to these findings, the IEEE 33-bus RDN has a minimum of approximately 60 % VAr compensation and a loss reduction of approximately 20%. Similarly, IEEE 69-bus RDN provides at least 40% VAr compensation, a 20% loss reduction, and net savings. Similarly, IEEE 85-bus RDN has a net savings of approximately 45% and a minimum VAr compensation of approximately 70%.

**Table 9**
*Performance of IEEE 33-bus with EV load after CBs allocation.*

| Parameter | Annual EV load growth (%) | | | | |
|---|---|---|---|---|---|
| | 10 | 20 | 30 | 40 | 50 |
| CB Sizes (kVAr) and locations | 1290 (6)<br>430 (31) | 635 (32)<br>425 (7)<br>740 (28) | 400 (23)<br>1085 (30)<br>370 (25) | 1020 (6)<br>795 (29)<br>65 (8) | 1460 (29)<br>10 (23)<br>690 (24) |
| kVAr Comp (%). | 69.92 | 68.55 | 66.81 | 64.39 | 70.70 |
| CB Cost ($)$_A$ | 466.66 | 491.05 | 539.54 | 584.50 | 560.32 |
| $P_{loss}$ (kW) | 171.0288 | 201.1701 | 233.1186 | 270.1779 | 309.9613 |
| $Q_{loss}$ (kVAr) | 115.3064 | 134.6747 | 156.285 | 180.6294 | 207.622 |
| $V_{min}$ (p.u.) | 0.917174 | 0.903339 | 0.902263 | 0.89242 | 0.9223 |
| VSI | 0.706805 | 0.665212 | 0.662181 | 0.633849 | 0.7226 |
| $P_{loss}$ Cost ($)$_B$ | 28732.83 | 33796.57 | 39163.92 | 45389.88 | 52073.51 |
| Total Cost ($)$_{A+B}$ | 29199.49 | 34287.63 | 39703.46 | 45974.38 | 52633.83 |
| % Savings | 26.57 | 25.15 | 23.86 | 21.77 | 19.85 |
| % $P_{loss}$ Reduction | 27.75 | 26.22 | 24.89 | 22.77 | 20.70 |

**Table 10**
*Performance of IEEE 69-bus with EV load after CBs allocation.*

| Parameter | Annual EV load growth (%) | | | | |
|---|---|---|---|---|---|
| | 10 | 20 | 30 | 40 | 50 |
| CB Sizes (kVAr) and locations | 75 (51)<br>1190 (62) | 990 (63)<br>770 (69)<br>65 (8) | 310 (8)<br>355 (7)<br>1490 (62) | 1555 (62)<br>355 (20) | 1150 (62)<br>390 (15)<br>45 (69) |
| kVAr Comp (%). | 43.99 | 59.83 | 66.96 | 56.50 | 44.81 |
| CB Cost ($)$_A$ | 233.80 | 344.52 | 393.07 | 394.97 | 311.34 |
| $P_{loss}$ (kW) | 183.8812 | 216.3134 | 250.6340 | 284.8726 | 321.6105 |
| $Q_{loss}$ (kVAr) | 85.4110 | 100.0357 | 116.0411 | 132.6704 | 150.0400 |
| $V_{min}$ (p.u.) | 0.9216 | 0.9140 | 0.9127 | 0.9056 | 0.8935 |
| VSI | 0.7193 | 0.6971 | 0.6931 | 0.6722 | 0.6370 |
| $P_{loss}$ Cost ($)$_B$ | 30892.04 | 36340.65 | 42106.52 | 47858.59 | 54030.56 |
| Total Cost ($)$_{A+B}$ | 31125.84 | 36685.16 | 42499.59 | 48253.56 | 54341.90 |
| % Savings | 29.03 | 26.94 | 25.23 | 24.25 | 23.25 |
| % $P_{loss}$ Reduction | 29.56 | 27.63 | 25.92 | 24.87 | 23.69 |

**Table 11**
*Performance of IEEE 85-bus with EV load after CBs allocation.*

| Parameter | Annual EV load growth (%) | | | | |
|---|---|---|---|---|---|
| | 10 | 20 | 30 | 40 | 50 |
| CB Sizes (kVAr) and locations | 150 (19)<br>600 (48)<br>1650 (8) | 600 (49)<br>1050 (11)<br>300 (62) | 450 (79)<br>600 (36)<br>1050 (11) | 900 (8)<br>750 (60)<br>450 (55) | 750 (51)<br>900 (63)<br>600 (11) |
| kVAr Comp (%). | 90.93 | 72.01 | 77.85 | 77.84 | 83.16 |
| CB Cost ($)$_A$ | 525.45 | 476.4 | 485.25 | 485.55 | 503.7 |
| $P_{loss}$ (kW) | 187.989 | 222.151 | 248.291 | 281.231 | 322.379 |
| $Q_{loss}$ (kVAr) | 115.065 | 137.188 | 154.226 | 173.397 | 197.014 |
| $V_{min}$ (p.u.) | 0.9171 | 0.9045 | 0.8988 | 0.8928 | 0.8947 |
| VSI | 0.7073 | 0.6693 | 0.6525 | 0.6354 | 0.6409 |
| $P_{loss}$ Cost ($)$_B$ | 31582.16 | 37321.36 | 41712.83 | 47246.80 | 54159.62 |
| Total Cost ($)$_{A+B}$ | 32107.61 | 37797.76 | 42198.08 | 47732.35 | 54663.32 |
| % Savings | 47.90 | 46.37 | 46.98 | 46.31 | 44.45 |
| % $P_{loss}$ Reduction | 48.76 | 47.05 | 47.58 | 46.85 | 44.96 |

## 7 Conclusion

An improved flower pollination algorithm (IFPA) is proposed in this study to address the issue of optimal CB allocation in RDNs, which has been reframed in view of the growing EV load penetration. The IFA has a dynamic switching probability and a double-direction learning technique built in to balance the exploration and exploitation phases as it moves toward the global optimum. The search space was reduced by selecting potential sites based on voltage stability indices (VSIs). The best locations and their sizes are then determined by the IFPA to minimize the real power losses and consequently maximize net savings and improve the voltage profile and voltage stability. Simulations were run on standard IEEE 33-, 69-, and 85-bus RDNs, and the results were compared to published research. Additionally, tests are expanded to cover a range of EV load penetration levels, and the benefits of placing ideal CBs in the right places are observed in terms of decreased losses, an improved voltage profile, increased voltage stability, and higher net savings.

However, the existing literature on CBs allocation and the results reported in this study fail to maintain the minimum voltage constraint. Even when the VAr compensation was set to 100 % (i.e., the VAr load was set to zero) in all three test systems, the voltage limitation was not satisfied. The distribution side's VAr adjustment and any corrective actions must maintain the voltage profile below ±5%. Based on this, the VAr compensation may not operate satisfactorily on its own. Additionally, according to voltage-dependent load modeling, electric vehicle loads are modeled as (battery charging); hence, the net effective EV load creates an additional network demand. Power quality issues were not addressed in this study because the simulations were run under balanced and steady-state

settings. In these areas, combined hybrid approaches are required, such as simultaneous DG, CB, and network reconfiguration, considering unbalanced loading conditions and power quality issues. These approaches may be considered in the future scope of this study.

## 8 Acknowledgments

The author wishes to thank the Department of Electrical and Electronics Engineering, School of Engineering and Technology, CHRIST (Deemed to be University), Karnataka, India, for the MATLAB computational facilities provided for conducting this research.

## 9 References

[1] G. Mokryani: Distribution Network Types and Configurations, Ch. 1, Future Distribution Networks: Planning, Operation, and Control, AIP Publishing, Melville, New York, 2022.

[2] H. Haes Alhelou, M. E. Hamedani-Golshan, T. C. Njenda, P. Siano: A Survey on Power System Blackout and Cascading Events: Research Motivations and Challenges, Energies, Vol. 12, No. 4, February 2019, p. 682.

[3] M. M. Aman, G. B. Jasmon, A. H. A. Bakar, H. Mokhlis, M. Karimi: Optimum Shunt Capacitor Placement in Distribution System – A Review and Comparative Study, Renewable and Sustainable Energy Reviews, Vol. 30, February 2014, pp. 429–439.

[4] H. A. Mahmoud Pesaran, P. D. Huy, V. K. Ramachandaramurthy: A Review of the Optimal Allocation of Distributed Generation: Objectives, Constraints, Methods, and Algorithms, Renewable and Sustainable Energy Reviews, Vol. 75, August 2017, pp. 293–312.

[5] S. Mishra, D. Das, S. Paul: A Comprehensive Review on Power Distribution Network Reconfiguration, Energy Systems, Vol. 8, No. 2, May 2017, pp. 227–284.

[6] S. K. Dash, S. Mishra, L. R. Pati, P. K. Satpathy: Optimal Allocation of Distributed Generators Using Metaheuristic Algorithms – An Up-to-Date Bibliographic Review, Proceedings of the 1st International Conference on Green Technology for Smart City and Society (GTSCS), Odisha, India, August 2020, pp. 553–561.

[7] Y. M. Shuaib, M. S. Kalavathi, C. C. Asir Rajan: Optimal Capacitor Placement in Radial Distribution System Using Gravitational Search Algorithm, International Journal of Electrical Power & Energy Systems, Vol. 64, January 2015, pp. 384–397.

[8] N. Gnanasekaran, S. Chandramohan, T. D. Sudhakar, P. S. Kumar: Maximum Cost Saving Approach for Optimal Capacitor Placement in Radial Distribution Systems Using Modified ABC Algorithm, International Journal on Electrical Engineering and Informatics, Vol. 7, No. 4, December 2015, pp. 665–678.

[9] V. Tamilselvan, K. Muthulakshmi, T. Jayabarathi: Optimal Capacitor Placement and Sizing in a Radial Distribution System Using Clonal Selection Algorithm, ARPN Journal of Engineering and Applied Sciences, Vol. 10, No. 8, May 2015, pp. 3304–3312.

[10] A. Y. Abdelaziz, E. S. Ali, S. M. Abd Elazim: Optimal Sizing and Locations of Capacitors in Radial Distribution Systems via Flower Pollination Optimization Algorithm and Power Loss Index, Engineering Science and Technology, an International Journal, Vol. 19, No. 1, March 2016, pp. 610–618.

[11] V. Tamilselvan, T. Jayabarathi, T. Raghunathan, X.- S. Yang: Optimal Capacitor Placement in Radial Distribution Systems Using Flower Pollination Algorithm, Alexandria Engineering Journal, Vol. 57, No. 4, December 2018, pp. 2775 – 2786.

[12] A. A. Abou El-Ela, R. A. El-Sehiemy, A. S. Abbas: Optimal Placement and Sizing of Distributed Generation and Capacitor Banks in Distribution Systems Using Water Cycle Algorithm, IEEE Systems Journal, Vol. 12, No. 4, December 2018, pp. 3629 – 3636.

[13] C. Kishore, S. Ghosh, V. Karar: Symmetric Fuzzy Logic and IBFOA Solutions for Optimal Position and Rating of Capacitors Allocated to Radial Distribution Networks, Energies, Vol. 11, No. 4, March 2018, p. 766.

[14] A. A. Zaki Diab, H. Rezk: Optimal Sizing and Placement of Capacitors in Radial Distribution Systems based on Grey Wolf, Dragonfly and Moth – Flame Optimization Algorithms, Iranian Journal of Science and Technology, Transactions of Electrical Engineering, Vol. 43, No. 1, March 2019, pp. 77 – 96.

[15] K. S. Sambaiah, T. Jayabarathi: Optimal Allocation of Renewable Distributed Generation and Capacitor Banks in Distribution Systems Using Salp Swarm Algorithm, International Journal of Renewable Energy Research, Vol. 9, No. 1, March 2019, pp. 96 – 107.

[16] P. T. Nguyen, T. Nguyen Anh, D. Vo Ngoc, T. Le Thanh: A Cost-Benefit Analysis of Capacitor Allocation Problem in Radial Distribution Networks Using an Improved Stochastic Fractal Search Algorithm, Complexity, Vol. 2020, December 2020, p. 8811674.

[17] M. W. Saddique, S. S. Haroon, S. Amin, A. R. Bhatti, I. Ali Sajjad, R. Liaqat: Optimal Placement and Sizing of Shunt Capacitors in Radial Distribution System Using Polar Bear Optimization Algorithm, Arabian Journal for Science and Engineering, Vol. 46, No. 2, February 2021, pp. 873 – 899.

[18] M. A. Elseify, S. Kamel, H. Abdel-Mawgoud, E. E. Elattar: A Novel Approach based on Honey Badger Algorithm for Optimal Allocation of Multiple DG and Capacitor in Radial Distribution Networks Considering Power Loss Sensitivity, Mathematics, Vol. 10, No. 12, June 2022, p. 2081.

[19] D. B. Prakash, C. Lakshminarayana: Optimal Siting of Capacitors in Radial Distribution Network Using Whale Optimization Algorithm, Alexandria Engineering Journal, Vol. 56, No. 4, December 2017, pp. 499 – 509.

[20] S. M. Abd Elazim, E. S. Ali: Optimal Locations and Sizing of Capacitors in Radial Distribution Systems Using Mine Blast Algorithm, Electrical Engineering, Vol. 100, No. 1, March 2018, pp. 1 – 9.

[21] K. R. Devabalaji, K. Ravi, D. P. Kothari: Optimal Location and Sizing of Capacitor Placement in Radial Distribution System Using Bacterial Foraging Optimization Algorithm, International Journal of Electrical Power & Energy Systems, Vol. 71, October 2015, pp. 383 – 390.

[22] S. P. Adam, S.- A. N. Alexandropoulos, P. M. Pardalos, M. N. Vrahatis: No Free Lunch Theorem: A Review, In: Approximation and Optimization, Springer Optimization and its Applications, Edited by I. C. Demetriou, P. M. Pardalos, Springer, Cham, Vol. 145, May 2019, pp. 57 – 82.

[23] X.- S. Yang: Flower Pollination Algorithm for Global Optimization, Proceedings of the 11th International Conference on Unconventional Computing and Natural Computation (UCNC), Lecture Notes in Computer Science, Orléans, France, September 2012, pp. 240 – 249.

[24] Z. A. A. Alyasseri, A. T. Khader, M. A. Al-Betar, M. A. Awadallah, X.- S. Yang: Variants of the Flower Pollination Algorithm: A Review, In: Nature-Inspired Algorithms and Applied

Optimization, Studies in Computational Intelligence, Edited by X.- S. Yang, Vol. 744, Springer, Cham, October 2018, pp. 91 – 118.

[25] X. Yang, Y. Shen: An Improved Flower Pollination Algorithm with Three Strategies and Its Applications, Neural Processing Letters, Vol. 51, No. 1, February 2020, pp. 675 – 695.

[26] U. K. Kumar, V. Janamala: Comparative Analysis of Load Flows and Voltage-Dependent Load Modeling Methods of Distribution Networks, Proceedings of the Congress on Intelligent Systems (CIS), New Delhi, India, September 2020, pp. 467 – 483.

[27] U. Eminoglu, M. H. Hocaoglu: Distribution Systems Forward/Backward Sweep-Based Power Flow Algorithms: A Review and Comparison Study, Electric Power Components and Systems, Vol. 37, No. 1, December 2008, pp. 91 – 110.

[28] D. Das, D. P. Kothari, A. Kalam: Simple and Efficient Method for Load Flow Solution of Radial Distribution Networks, International Journal of Electrical Power and Energy Systems, Vol. 17, No. 5, October 1995, pp. 335 – 346.

[29] M. Chakravorty, D. Das: Voltage Stability Analysis of Radial Distribution Networks, International Journal of Electrical Power & Energy Systems, Vol. 23, No. 2, February 2001, pp. 129 – 135.

[30] M. E. Baran, F. F. Wu: Network Reconfiguration in Distribution Systems for Loss Reduction and Load Balancing, IEEE Transactions on Power Delivery, Vol. 4, No. 2, April 1989, pp. 1401 – 1407.

[31] M. E. Baran, F. F. Wu: Optimal Capacitor Placement on Radial Distribution Systems, IEEE Transactions on Power Delivery, Vol. 4, No. 1, January 1989, pp. 725 – 734.